International Journal of Heat and Mass Transfer 236 (2025) 126384

Contents lists available at ScienceDirect

International Journal of Heat and Mass Transfer

journal homepage: www.elsevier.com/locate/hmt

Experimental investigation of the performance of a phase change material thermal management module under vacuum and atmospheric pressure conditions

Laryssa Sueza Raffa [a,*], Matt Ryall [b], Nick S. Bennett [a], Lee Clemon [a,c]

[a] School of Mechanical and Mechatronic Engineering, University of Technology Sydney, Ultimo, NSW 2007, Australia
[b] Mawson Rovers, Eveleigh, NSW 2015, Australia
[c] Mechanical Science and Engineering, University of Illinois, Urbana, IL 61801, USA

ARTICLE INFO

Keywords:
Experiment
Heat sink
Phase change materials (PCMs)
Thermal management
Vacuum

ABSTRACT

High computational power and miniaturisation of modern electronics lead to high heat generation, compounded by the decreased available area for heat dissipation. This challenge is exacerbated in space environments due to the lack of convection. Phase change materials (PCM) are a strong option for the passive thermal management of satellites. However, their behaviour in vacuum is unclear. This study experimentally investigates and compares the performance of non-PCM and PCM-based thermal control modules under atmospheric pressure and vacuum conditions. A stainless steel heat sink with internal planar fins was tested using a printed circuit board (PCB) to produce three input power levels, simulating the heat dissipated by satellite electronics. Paraffin wax was used as the PCM. The thermal performance is reported and analysed for both pressure conditions. A reduced-order numerical model was established to predict performance with low required computational effort. This work finds that electronics operating in vacuum displayed temperatures as much as 32.8% higher compared to those in atmosphere due to decreased heat dissipation resulting from the lack of convective heat transfer. In addition, PCM had a greater impact in reducing the electronics temperature in vacuum than at atmospheric pressure. The presence of 6 g of PCM lowered the electronics temperatures by up to 18.0 °C in vacuum, and by up to 12.3 °C in atmospheric pressure. That amount of PCM doubled the electronics operating time under both pressure conditions at high power. The findings of this work contribute to understanding the performance variances of non-PCM and PCM-based heat sinks under different pressure conditions to further improve the design of thermal management modules for satellites.

1. Introduction

The modernisation of electronics, characterised by increased computational power and miniaturisation of the devices, leads to significantly higher heat generation, compounded by the decreased available area for heat dissipation [1–3]. This challenge is exacerbated in space environments, where the absence of air impedes heat transfer via convection. The imminent risk of overheating the avionics and subsystems of spacecrafts and satellites poses a critical threat to mission success. Therefore, effective thermal management strategies are paramount to ensure the reliability and longevity of electronic components in these demanding operational conditions and unique environments [4].

Thermal management systems may be active or passive. Active systems rely on moving parts to promote cooling through forced fluid convection. Their disadvantages for satellite applications are the additional power consumption and high maintenance. Passive thermal management systems have been increasingly studied as a preferred alternative for cooling small satellites due to their reduced operational complexity and absence of power requirement [5–7]. These systems include thermal louvres, heat pipes and phase change materials (PCMs). The use of PCM-based thermal energy storage units for satellites has attracted considerable attention in recent years, owing to their high heat absorption at constant temperatures and suitability to systems with intermittent heat dissipation [8–12]. Solid–liquid PCMs predominate due to their relatively low thermal expansion and chemical stability at repeated cycles [13,14]. PCMs use their high latent heat of fusion to absorb the thermal energy dissipated from the electronics, maintaining these electronics below their maximum allowable working temperature. When the avionics enter idle mode, the stored thermal energy is released to the surroundings as the PCM solidifies, in preparation for the next cycle. Another advantage of using PCMs for the thermal

* Corresponding author.
E-mail address: laryssa.suezaraffa@uts.edu.au (L. Sueza Raffa).

https://doi.org/10.1016/j.ijheatmasstransfer.2024.126384
Received 14 August 2024; Received in revised form 4 October 2024; Accepted 27 October 2024
Available online 8 November 2024
0017-9310/© 2024 The Authors. Published by Elsevier Ltd. This is an open access article under the CC BY license (http://creativecommons.org/licenses/by/4.0/).

Nomenclature

English symbols

A_{sec}	Cross-sectional area (m^2)
C_p	Specific heat capacity (J/kg K)
g	Gravitational acceleration (9.8 m/s^2)
H	Latent heat (J/kg)
k_{equiv}	Equivalent thermal conductivity (W/m K)
L	Heat sink height (m)
m	Mass (kg)
P	Power input (W)
p	Pressure (Pa)
Q	Thermal energy (J)
R	Heater trace resistance (Ω)
T	Temperature (°C)
t	Time (s)
T_l	Liquidus temperature of PCM (°C)
T_s	Solidus temperature of PCM (°C)
u, v, w	Velocities in x, y, and z-direction
U	Voltage (V)

Greek symbols

β	Volumetric thermal expansion coefficient (K^{-1})
μ	Dynamic viscosity (Kg/m s)
ρ	Density (kg/m^3)

Subscripts

$s-s$	Steady-state
$equiv$	Equivalent
top	Referent to the heat sink's top surface
$base$	Referent to the heat sink's base surface
$sens$	Sensible
lat	Latent
HS	Heat sink
PCM	Phase change material
∞	Surroundings

management of satellites is their behaviour as a thermal buffer. This allows the design of heat rejection modules for the average thermal load, as PCMs store thermal energy at peak load by changing phase and dissipate it to the surroundings afterward [5,15].

One notable drawback of PCMs is their relatively low thermal conductivity, which could delay heat transfer from the electronics into the PCM and to the surroundings. To address this limitation, various solutions have been explored, including the incorporation of thermal conductivity enhancers, such as the addition of metallic fins, porous structures [10,16,17], and the dispersion of nanoparticles within the PCM-based heat sinks [18]. Bose and Amirtham [19] provide a thorough review of methods for enhancing the thermal conductivity of paraffin wax in latent heat storage systems. Metallic fins have been extensively studied to improve the heat transfer within the PCM. Ye et al. [20] and Zhang et al. [21] provide a detailed overview of fin types and parameters investigated in the literature. The vast majority of these investigations on PCM-based finned heat sinks were conducted exclusively under atmospheric pressure conditions [16,22–31]. Therefore, the behaviour of PCM-based thermal control modules under vacuum conditions is not well documented.

Guo et al. [32] contributed to elucidating the topic by reporting the results of experiments with a 3D-printed lattice structure with N-tetradecane PCM in a vacuum chamber. The study analysed the transient temperature profiles under different initial temperatures and concluded that the PCM-based heat sink significantly enhanced thermal performance by improving heat transfer rates and maintaining stable temperatures. Initial temperatures were reported to have a slight effect on the thermal storage performance. Elshaer et al. [33] conducted a numerical investigation of open-cell copper foam with PCM in a thermal vacuum chamber. Two different porosities of the metal foam were studied at heating power levels of 7 W and 10 W. The study predicts the reduction in the maximum temperature of the thermal management module upon the addition of a PCM. Elshaer et al. [34] numerically investigated the effect of multiple fin geometries in an aluminium heat sink with organic PCM. The simulation disregarded convection heat transfer to simulate a space environment, and considered different types of fins, namely parallel fins, cross fins and pin fins. Triangular pin fins showed superior thermal performance for the setup developed in the study. In addition, the number of pin fins was observed to be directly related to the performance of the heat sink. Other research indirectly studied the operation of thermal management modules in vacuum, by focusing on the effects of microgravity on heat transfer through numerical simulation. Kansara et al. [35] numerically studied the effect of microgravity on a pin-finned heat sink with PCM. The research focused on the microgravity effect on the internal behaviour of the thermal control module, namely the melting and solidification processes of the PCM. Convective and radiative heat dissipation to the surroundings were disregarded. The study concluded that gravity has a strong influence during melting of the PCM, with the liquid fraction decreasing by 18% for a gravitational acceleration of g/80. In addition, natural convection seemed not to be dominant during the solidification process. A numerical analysis of a PCM-based thermal storage heat sink for thermal control of satellites was performed by Elshaer [36]. The study investigated the effect of PCM melting point and of PCM combinations on the thermal performance of the heat sink under microgravity, with no natural convection. The presence of PCM improved the thermal performance of the heat sink, leading to a maximum temperature decrease of 34.6%. PCM melting point was reported to be a dominant factor in the performance of the heat sink, with the more effective PCM combinations being between PCMs of differing melting points. While these numerical studies divulge the behaviour of PCM heat sinks in vacuum or low gravity conditions, the difference in the performance of PCM-based thermal management modules under atmospheric pressure and vacuum conditions remains unclear, especially experimental.

Understanding the behaviour of PCM-based heat sinks in vacuum is relevant for the fast-growing space industry. Most experimental studies on the performance of PCM-based thermal management modules have been performed for atmospheric pressure, including parametric analysis, different types of PCM, among others. The influence of these parameters on heat sink performance is well understood for atmospheric pressure. For vacuum conditions, however, there are limited studies on the performance of PCM-based heat sinks, which highlights the need to quantify the performance difference under both pressure conditions. Moreover, the fact that most of the existing studies have been limited to simulation shows a clear necessity for experimental investigation in vacuum conditions.

The present study aims to compare the performance of PCM-based thermal management modules under vacuum and atmospheric pressure conditions. Experimental tests were conducted for two thermal control samples: a stainless steel heat sink with plane fins without PCM, and the same heat sink with paraffin wax as a PCM. In addition, a simplified numerical model was developed to enable the prediction of the performance of PCM-based heat sinks under both pressure conditions. The reduced-order numerical model simplifies the heat sink and the PCM to a homogeneous solid with an equivalent thermal conductivity determined experimentally. Similar approaches have sought to reduce computational time. Gopalan and Eswaran [17] utilised the equivalent

thermal conductivity of a structured porous media cell to determine the optimum quantity of PCM in two types of heat sinks. The study concludes that the effectiveness of the heat sink is primarily determined by the equivalent thermal conductivity, irrespective of the porosity of the porous media structure or the type of thermal conductivity enhancer utilised. Guo et al. [32] also employed the concept of equivalent thermal conductivity onto a PCM-based lattice structured thermal energy storage device. This style of model is adopted in this study and compared to the experimental results. The novelty of the work is listed below:

- Experimental quantification of the performance differences of a PCM-based thermal management module operating under vacuum and atmospheric pressure conditions.
- Development of a reduced order numerical model to predict the performance of thermal management modules under both pressure conditions that demand reduced computational time.

The findings here add to the existing literature regarding the optimisation of thermal conductivity enhancers under atmospheric pressure conditions and have the potential to guide required design modifications to ensure a tailored solution for space conditions.

2. Methodology

2.1. Experimental study

The present study compares the performance of a passive thermal management module under vacuum and atmospheric pressure conditions. The heat sink was mounted on top of a flat electric heater, which simulated the heat emitted by the electronics in a satellite. The temperature at the base of the heat sink was monitored throughout the heating and cooling cycle at 5-s intervals. The temperature at the base of the heat sink coincides with the electronics temperature in this experiment and, therefore, is indicative of the performance of the thermal management module. In other words, lower base temperatures indicate that thermal energy is dissipated away from the electronics more effectively by being absorbed by the heat sink during heating. The temperature at the top of the heat sink is also monitored to provide insight into the heat transfer through the heat sink and the heat rejection to the surroundings.

2.1.1. Thermal management module

The thermal management module for the present research is comprised of the heat sink shown in Fig. 1. The heat sink was manufactured in stainless steel SS316L via laser powder bed fusion with a GE Concept Laser M2 series 5 machine and was 3D-printed in one piece, including its four mounting feet and internal vertical plane fins. It has two holes at the top surface for powder removal and injection of PCM. The heat sink weighs 150.0 g, and its dimensions are 30 mm wide, 30 mm deep and 37 mm high. Testing was conducted for an empty heat sink and for the heat sink filled in with PCM.

For the case with PCM, an organic solid–liquid PCM was selected for its high energy density, stable physical and chemical properties, and uniform melting properties. To meet the desired operational requirements for the experiments, the Sigma-Aldrich 327 204 paraffin wax was selected. The melting point of this material ranges from 53 to 58 °C. The preparation of the PCM-based thermal management module for the experiments is as follows. Liquid paraffin was poured into the internal cavity of the heat sink through the top holes. To eliminate the risk of leakages during thermal expansion, the liquid PCM occupies approximately 70% of the heat sink's available internal volume, which results in 6.0 g of paraffin. This void space allows the paraffin's expansion during phase change, especially under vacuum conditions, where it was observed that the paraffin expansion rate is larger than that at standard atmospheric pressure. The paraffin injection holes were sealed with O-rings and screws. The module was completely cooled down to room temperature before each experiment.

2.1.2. Experimental setup

Figs. 2(a) and 2(b) show the experimental setup for the present study and its schematic diagram. The components of the test rig are mainly a battery-operated printed circuit board (PCB) and a microprocessor. The BeagleBone Black microprocessor collects and processes the temperature data from the thermistors. The data is transmitted wirelessly into a web-based control dashboard, which displays it in real-time, stores it in a web cloud system, and enables control of the heater.

The printed circuit board (PCB) and its software were custom-made by the Australian company and industry partner Mawson Rovers. The PCB has a 30 × 30 mm circuit-printed copper heater that provides uniform heating to the base of the heat sink, which is mounted onto the heater. The PCB contains two thermistors to monitor the temperature of the heat sink. One thermistor was soldered at the centre of the heater to measure the temperatures at the base of the heat sink, while the other one was adhered to the top of the heat sink with tape. The make and model of the soldered and top thermistors is Vishay NTCS0603E3103FMT and Vishay NTCALUG01A103FLA, respectively. The measurement uncertainty of both thermistors was ±1%. The temperature readings were obtained every 5 s and collated by the BeagleBone.

The heater signals are pulsed width modulation (PWM) type. In this study, experiments were conducted at three power levels: high (100% duty), medium (50% duty), and low (30% duty). At 100% duty, the heater is constantly on, while at lower duties, it alternates between on and off states in direct proportion to the duty cycle, delivering reduced average power as shown in Eq. (1). The power input at 100% duty ($P_{100\%duty}$) was determined with the PCB voltage (U), and the resistance across heater (R) by Eq. (2). Both the voltage and resistance were measured with a multimeter, with an uncertainty of ±1.5% and ±0.5%, respectively. The measured voltage was 4.5 V. The resistance, R was measured for various temperatures to determine its correlation as a function of temperature T (Eq. (3)).

$$P = P_{100\%duty} * (Duty) \tag{1}$$

$$P_{100\%duty} = \frac{U^2}{R} \tag{2}$$

$$R = 0.015T + 1.99 \tag{3}$$

Eq. (1) yields temperature-dependent power inputs that range from 8.4–5.7 W for high heat (100% duty), 4.2–3.1 W for medium heat (50% duty), and 2.5–2.0 W for low heat (30% duty). These power input ranges are referent to the temperatures at the start and at the end of the heating process. The initial temperature of each test was kept within tolerance of 23 °C ± 1.5 °C.

The test rig and the thermal management module were tested under atmospheric pressure and vacuum conditions. In the experiments performed under vacuum conditions, a vacuum pump sustained the pressure in the chamber at 5 Pa to approximate the test conditions to the space environment. The ambient temperature was kept at 23 °C ± 1.5 °C throughout all the experiments.

2.1.3. Uncertainly analysis

The uncertainty in the measurement of the quantities utilised in this work is listed in Table 1. The uncertainty in power $P = \frac{U^2}{R}$ was calculated from the independent variables voltage and resistance for the worst case scenario observed during the experiments, specifically maximum voltage (4.5 V) and minimum resistance (2.33 Ω at initial temperature):

$$\delta_P = \sqrt{\left(\frac{\partial P}{\partial U}\cdot\sigma_U\right)^2 + \left(\frac{\partial P}{\partial R}\cdot\sigma_R\right)^2} = \sqrt{\left(\frac{2U}{R}\cdot\sigma_U\right)^2 + \left(-\frac{U^2}{R^2}\cdot\sigma_R\right)^2} \tag{4}$$

2.1.4. Test procedure

To reduce the contact resistance between the surface of the heater and the bottom surface of the heat sink, a coating of Apiezon H thermal

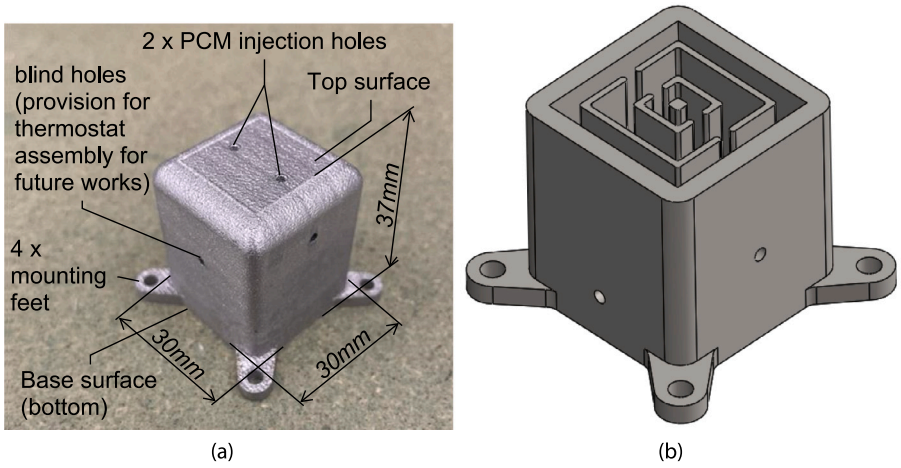

Fig. 1. Picture of the heat sink utilised in the experiments (a) and section view of CAD drawing (b).

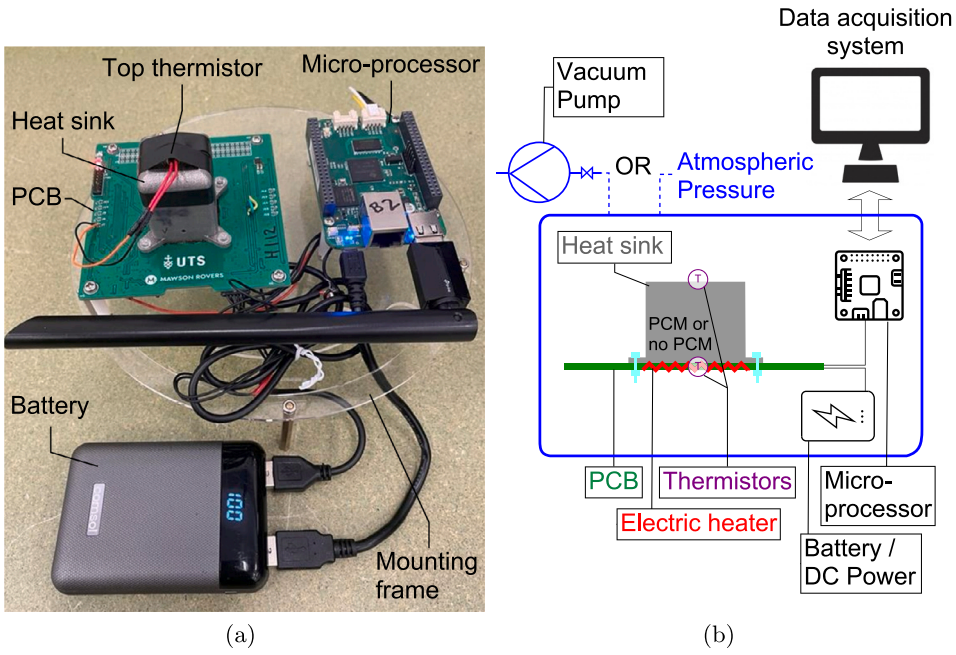

Fig. 2. Experimental set up picture (a) and schematic (b).

Table 1
Results of the uncertainty analysis.

Parameter	Instrument	Uncertainty %	Uncertainty σ
Voltage	Multimeter	±1.5%	±0.07 V
Resistance	Multimeter	±0.5%	±0.01 Ω
Temperature	Thermistor	±1.0%	±0.25–1 °C
Power	Dependent variable	±3.1%	±0.27 W

grease was applied between these surfaces. The heat sink was then assembled onto the PCB and secured with nylon bolts and nuts to minimise heat dissipation through the fixings into the other areas of the PCB. Each test was initialised with the system completely cooled down to 23 °C ± 1.5 °C. The heater was then switched on at the desired power setting and was programmed to turn off after 90 min or when the base of the heat sink reached 100 °C, whichever occurred first. The 100 °C peak temperature was set to avoid overheating the electronics of the PCB, as recommended by the manufacturer. The system was then left to cool. The thermistors at the top and the base of the heat sink measured the temperatures at these locations at 5-s intervals throughout the heating and cooling processes. The temperature over time graphs were plotted for each test in Section 3.

Table 2
Variations of the experimental tests.

Test variation	Test condition	PCM mass (g)	Power input
1	Atmospheric pressure	–	Low
2	Atmospheric pressure	–	Medium
3	Atmospheric pressure	–	High
4	Atmospheric pressure	6.0	Low
5	Atmospheric pressure	6.0	Medium
6	Atmospheric pressure	6.0	High
7	Vacuum	–	Low
8	Vacuum	–	Medium
9	Vacuum	–	High
10	Vacuum	6.0	Low
11	Vacuum	6.0	Medium
12	Vacuum	6.0	High

A full factorial test series was conducted for the variables of interest, as summarised in Table 2.

2.2. Reduced order numerical model

A reduced-order numerical model was developed to predict the performance of heat sinks operating under atmospheric pressure and vacuum conditions. The experimental results were used to verify the applicability of the low-complexity model as a quick estimator to compare the operation of heat sinks under different conditions.

This model assumes a homogeneous solid with lumped mass and equivalent thermal conductivity. Similar approaches have been used in the literature to reduce computational efforts [17,32]. The equivalent thermal conductivity was determined experimentally for the "No PCM" and "PCM" cases.

Determining effective thermal conductivity. We assume the heat sink consists of a homogeneous solid with external dimensions matching the design and with an equivalent thermal conductivity measured experimentally, as follows. The heat sink was placed onto the PCB described in Section 2.1.2. The side walls of the heat sink were insulated with thermal insulating foam. The heater was turned on at a defined heater power level until the heat sink reached steady-state, when both the bottom and the top temperatures plateaued. In steady-state, the heat that enters the system leaves it at the same rate and therefore the heat sink no longer stores thermal energy. The equivalent thermal conductivity k_{equiv} was then calculated from Fourier's law of heat conduction (Eqs. (5) and (6)). This process was performed for the cases without PCM and with PCM to determine the effective thermal conductivity of both samples. For the heat sink with PCM, the process was performed at different power levels in a piece-wise manner to cater for the distinct thermal conductivity of liquid and solid PCM.

$$P_{s-s} = -k_{equiv} A_{sec} \frac{(T_{top,s-s} - T_{base,s-s})}{L} \tag{5}$$

$$k_{equiv} = \frac{P_{s-s} L}{A_{sec}(T_{base,s-s} - T_{top,s-s})} \tag{6}$$

where P_{s-s} is the heat input (W) at steady-state, k_{equiv} is the equivalent thermal conductivity of the sample (W/m K), A_{sec} is the cross-sectional area of the heat sink (m^2), $T_{top,s-s}$ and $T_{base,s-s}$ are the temperatures at the top and at the base of the heat sink (°C) in steady-state, and L is the height of the heat sink (m).

Thermal simulation using reduced-order model. The numerical simulations were performed utilising the finite element method through ANSYS Fluent 2021. An equivalent material was created for each sample with the equivalent thermal conductivity obtained from experimental data using Eq. (6). The density of the created materials was defined using the volume-based rule of mixtures and the properties of stainless steel and paraffin wax, as shown in Table 3.

The specific heat capacity for the heat sink without PCM was taken as that of stainless steel. For the heat sink with PCM, the latent heat of the paraffin was represented as a large specific heat capacity between the PCM melting range, consistent with related prior works [11,37,38]. The specific heat capacity of the composite material exhibits three different levels: below the PCM melting range, between the PCM melting range, and above it. Outside of the PCM melting range, the equivalent specific heat capacity was determined using a volume-based rule of mixtures between stainless steel and paraffin wax. Between the melting range of the PCM, the equivalent specific heat capacity incorporates the total latent heat capacity of the paraffin quantity as a single value as shown in Eqs. (7)–(8). The thermal energy absorbed by the composite solid during PCM phase change Q_{equiv} is composed of the sensible heat absorbed by the stainless steel heat sink $Q_{HS,sens}$, and the sensible and latent heat absorbed by the PCM, $Q_{PCM,sens}$ and $Q_{PCM,lat}$. The use of the specific heat capacity to proxy the latent heat storage captures the effect of thermal storage in the material without employing a multi-phase multi-physics simulation, greatly reducing the computational cost and time. Due to the simplifications applied in the proposed numerical model, the dynamics of liquid fraction were not included in this work.

Table 3
Material properties adopted in this study [31,39].

Material	Density (kg/m^3)	Melting point (°C)	Specific heat capacity C_p (J/kg K)	Latent heat capacity H (J/kg)
Stainless steel SS316L	8000	–	500	–
Paraffin wax	880	53–58	2000	170 000

$$Q_{equiv} = Q_{HS,sens} + Q_{PCM,sens} + Q_{PCM,lat} \tag{7}$$

$$m_{equiv} C_{p_{equiv}} (T_l - T_s) = m_{HS} C_{p_{HS}} (T_l - T_s) + m_{PCM} C_{p_{PCM}} (T_l - T_s) + m_{PCM} H_{PCM} \tag{8}$$

where T_l and T_s are the liquidus and solidus temperature of the PCM, $C_{p_{equiv}}$ is the equivalent specific heat capacity for the heat sink with PCM case within the phase change temperature range, and H_{PCM} is the latent heat capacity of the PCM (170 000 J/kg). It was assumed for Eqs. (7) and (8) that the heat sink and PCM are at the same temperature and that the totality of the PCM changes phase between T_l and T_s. Eq. (8) was then solved for $C_{p_{equiv}}$ to find the equivalent specific heat capacity for the case with PCM.

For the simulations under atmospheric pressure, the surrounding air was considered an incompressible fluid with null forced airflow velocity which allows for natural convection. For the vacuum simulations, the operating pressure was adjusted to 5 Pa to reproduce the internal pressure of the vacuum chamber utilised in the experiments (i.e low-grade vacuum). In addition to the radiation heat transfer, a minimal convection heat transfer coefficient was applied to the walls' boundary conditions to accommodate the remaining internal pressure of the experimental vacuum chamber. The adopted thermal emissivity for the heat sink walls was 0.6, adapted from [40] due to the high surface roughness from the laser powder bed fusion manufacturing process.

The governing equations for the transient thermal simulations solved by Ansys are [33,41]:

$$\frac{\delta u}{\delta x} + \frac{\delta v}{\delta y} + \frac{\delta w}{\delta z} = 0 \tag{9}$$

$$\rho\left(\frac{\delta u}{\delta t} + \frac{\delta u}{\delta x} + \frac{\delta u}{\delta y} + \frac{\delta u}{\delta z}\right) = -\frac{\delta p}{\delta x} + \mu\left(\frac{\delta^2 u}{\delta x^2} + \frac{\delta^2 u}{\delta y^2} + \frac{\delta^2 u}{\delta z^2}\right) \tag{10}$$

$$\rho\left(\frac{\delta v}{\delta t} + \frac{\delta v}{\delta x} + \frac{\delta v}{\delta y} + \frac{\delta v}{\delta z}\right) = \rho g \beta (T - T_\infty) + \mu\left(\frac{\delta^2 v}{\delta x^2} + \frac{\delta^2 v}{\delta y^2} + \frac{\delta^2 v}{\delta z^2}\right) \tag{11}$$

$$\rho\left(\frac{\delta w}{\delta t} + \frac{\delta w}{\delta x} + \frac{\delta w}{\delta y} + \frac{\delta w}{\delta z}\right) = -\frac{\delta p}{\delta w} + \mu\left(\frac{\delta^2 w}{\delta x^2} + \frac{\delta^2 w}{\delta y^2} + \frac{\delta^2 w}{\delta z^2}\right) \tag{12}$$

We then substitute our effective composite material properties into Eq. (13).

$$\rho_{equiv} C_{p_{equiv}} \frac{\delta T}{\delta t} = k_{equiv}\left(\frac{\delta^2 T}{\delta x^2} + \frac{\delta^2 T}{\delta y^2} + \frac{\delta^2 T}{\delta z^2}\right) \tag{13}$$

where u, v, w are the velocity components in x, y, z directions, ρ is the density, p is the pressure, g is the gravitational acceleration, β is the volumetric thermal expansion coefficient, μ is the viscosity, and T is the temperature. Where ρ_{equic}, C_{p_equiv} and k_{equiv} refer to the density, specific heat capacity and thermal conductivity for the equivalent materials created for the cases "without PCM" and "PCM".

The initial and boundary conditions are outlined as follows and illustrated in Fig. 3:

1. The simulations were initialised at 23 °C.
2. Heat flux with the heater at high power was applied onto the base surface of the heat sink during heating and used the correlation of heat flux as a function of the temperature as described in Section 2.1.2.

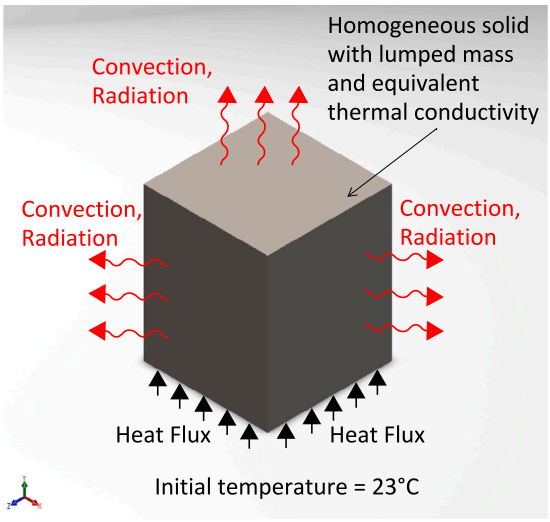

Fig. 3. Initial and boundary conditions of the reduced-order numerical model.

3. Heat transfer through the walls and top surface of the heat sink was considered via natural convection and radiation for both the atmospheric pressure and vacuum simulations, such that a minimum convection heat transfer coefficient was adopted for vacuum to accommodate the remaining 5 Pa of internal pressure of the experimental vacuum chamber.

The numerical simulations were compared to the experimental data to validate the reduced-order method; comparisons are discussed in Section 3.2.

3. Results

3.1. Experimental work

3.1.1. Atmospheric pressure transient temperatures

The heat sink without and with PCM was heated at low, medium and high power levels for 90 min (5400 s) or upon reaching 100 °C, whichever came first. The heating process for the atmospheric pressure tests at all power levels lasted 5400 s, since the base temperatures did not reach 100 °C. The effectiveness of PCM in maintaining lower electronics temperatures can be examined by comparing the base temperatures for the cases with and without PCM. The addition of PCM consistently lowered the electronics temperature during the heating process across all power levels, as shown in Fig. 4. This is attributed to the additional thermal energy stored by the PCM across three phases: pre-fusion, fusion/melting, and post-fusion. As expected, the fusion/melting phase is responsible for the bulk of the additional heat stored due to the material/s latent heat of fusion. Nevertheless, the impact of PCM in minimising temperature is evident early in the transient curves, when the base temperature is at around 35 °C for the low power case, around 40 °C for medium power, and around 45 °C for high power case.

During the heating process, the heat sink without PCM achieved a maximum base temperature of 52.0 °C, 64.6 °C and 97.2 °C for low, medium and high power, respectively. The addition of PCM lowered the maximum temperatures by 2.0 °C for low and medium power, and 4.5 °C for high power. Therefore, the reduction in the maximum temperature was more significant for high power input, at 4.6%. In comparison, the decrease was 3.8% for low heat and 3.1% for medium heat. In the cooling phase, the base temperatures were higher for a longer period of time with PCM. This was expected due to the extra energy stored by the PCM during heating, both sensible and latent, which was gradually released during cooling.

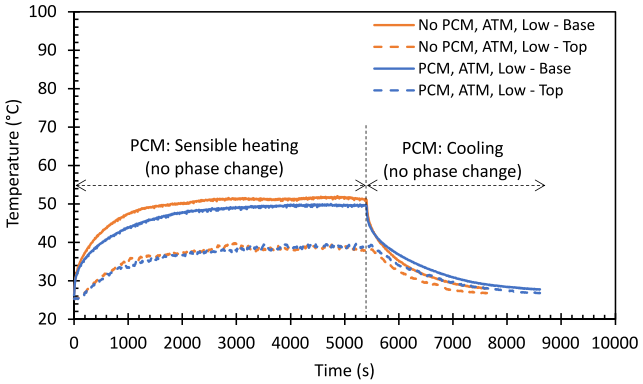

(a) ATM - Low power

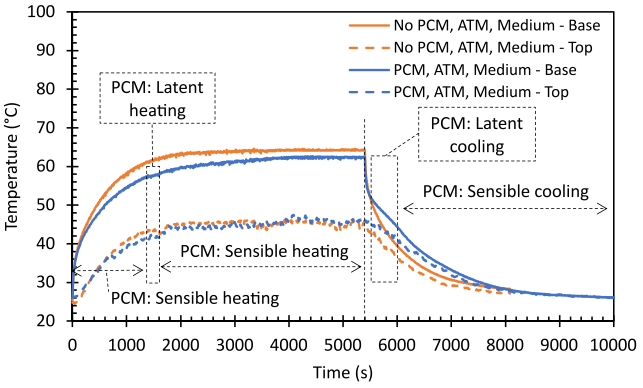

(b) ATM - Medium power

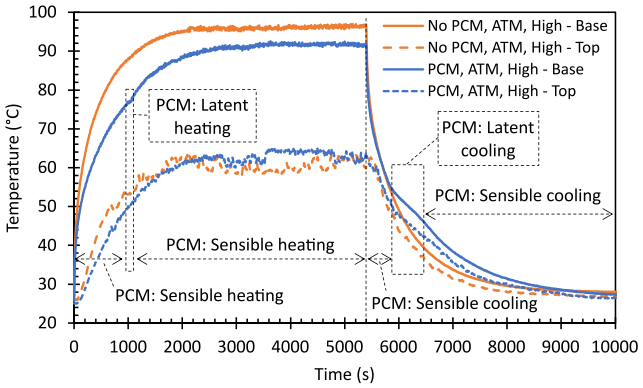

(c) ATM - High power

Fig. 4. Transient temperatures for experiments conducted under atmospheric pressure for heat sinks with and without PCM. Temperatures at the base and top surfaces of the heat sink at low (a), medium (b), and high (c) power levels.

PCMs change phase at a constant temperature. Hence the melting and solidification periods of PCM can be pinpointed in the transient graphs as the periods of nearly constant temperature. Phase change was observed in both the medium and high power experiments. Figs. 4(b) and 4(c) show a short period of nearly constant base temperatures during heating, indicative of paraffin melting, at around 57.0 °C for medium power and 77.0 °C for high power, roughly at 1500 s and 1000 s, respectively. It is important to note, however, that the maximum top temperature for medium power was 47.5 °C, which is below the paraffin melting point. This suggests that, unlike the high-power input experiment, some of the PCM may not have melted at medium

heat input. Stable temperatures were also present during the cooling phase, with the onset of solidification at around 53 °C in both medium and high power tests. In contrast, it can be observed that no phase change occurred in the low-power input test (i.e no nearly constant temperatures during heating or cooling). This affirmation is reinforced by the observation in Fig. 4(a), that neither the base nor the top of the heat sink reached the melting point of the PCM.

3.1.2. Vacuum pressure transient temperatures

The vacuum tests with PCM yielded lower temperatures at the base of the heat sink throughout the heating phase for all power levels compared to "No PCM", as observed in Fig. 5. This is consistent with the tests in atmospheric pressure. The effect of PCM in lowering the base temperature is also visible early in the curves, from around 30 °C for low heat, 35 °C for medium heat, and 45 °C for high power level. At low heat input, Fig. 5(a) shows that the maximum base temperature was reduced from 65.2 °C to 60.9 °C with the addition of PCM. This difference of 4.3 °C represents a reduction of 6.7%. Similarly, at medium power level, the temperature was reduced by 3.7 °C, or 4.3% (Fig. 5(b)). Fig. 5(c) displays the results for high power experiments, in which the heating process was halted upon reaching 100 °C for both cases. This limit was required to protect the circuitry by ensuring the heater-thermostat module remained below its maximum allowable working temperature set by the manufacturer. It was observed that the case with PCM was able to operate significantly longer than without PCM. The case with PCM reached 100 C after 1570 s, which is 60.7% longer than the case without PCM (977 s). As expected during cooling, cases with PCM maintained higher temperatures longer due to the release of the extra energy stored by the PCM. The slower cooling rate begins when the PCM nears the solidification temperature and extends the lower temperature cool down time below the solidus temperature.

Phase change of the PCM was observed for all power levels. At low power input, although a stabilisation in temperature is not obvious during heating, it is noticeable during the cool down phase, when the base of the heat sink is at around 54 °C as shown in Fig. 5(a). The maximum temperature at the top surface is only 52.3 °C, which is below the PCM melting range of 53 to 58 °C. This indicates that the low power input was insufficient to melt the totality of PCM contained in the heat sink. PCM fusion is observed when the base temperature is between 60 to 68 °C for medium power, and at around 77 °C for high power. Figs. 4(b) and 5(c) also show that the top temperatures surpassed the paraffin's melting point for these two power levels, which indicates that the entire volume of paraffin within the heat sink changed phase. The onset of solidification consistently occurs at the same temperature for all power levels, when the base of the heat sink is at around 54 °C.

3.2. Reduced order model

A reduced-order numerical model was developed to predict the performance of heat sinks in both atmospheric and vacuum conditions with low computational power requirements. The validation of the reduced order numerical model is shown in Fig. 6. The model shows good agreement for both "No PCM" and "PCM" cases under atmospheric pressure and vacuum conditions. The reduced order model predicts slightly higher steady-state temperatures and is, therefore, slightly conservative for this heat sink design.

For the cases under atmospheric pressure (Fig. 6(a)), a good agreement between the experimental data and the numerical model was observed for the base temperatures. The maximum difference between the simulation and the experiment is observed within the first few minutes of heating for the "No PCM" case, at 4.2 °C. For the case with PCM, the maximum difference between numerical model and experiment is 4.7 °C and occurred around the phase change period of the material, as expected due to the model being based on the equivalent thermal conductivity and equivalent specific heat capacity.

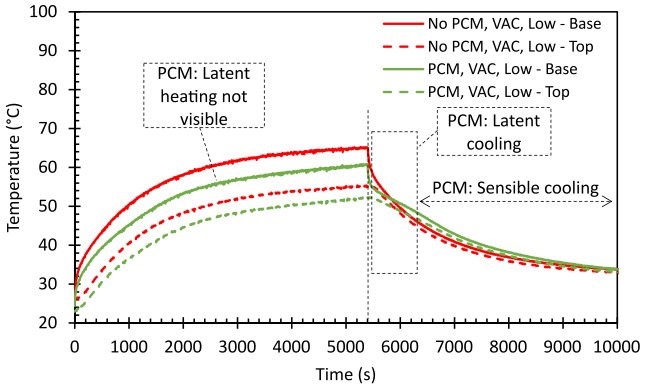

(a) VAC - Low power

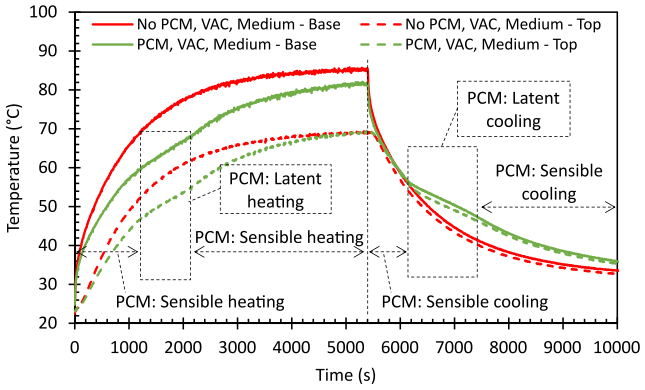

(b) VAC - Medium power

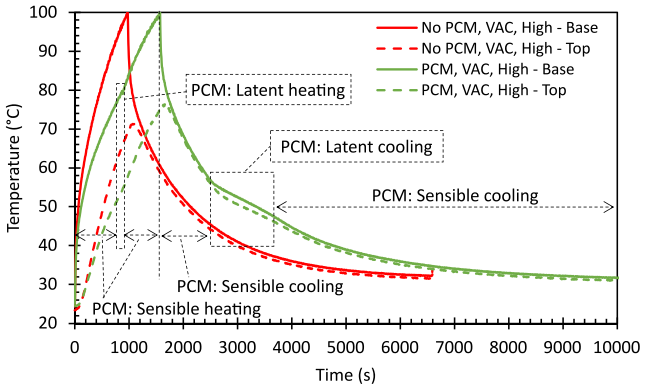

(c) VAC - High power

Fig. 5. Transient temperatures for experiments conducted under vacuum for heat sinks with and without PCM. Temperatures at the base and top surfaces of the heat sink at low (a), medium (b), and high (c) power levels.

In other words, the numerical model considers that the equivalent solid has the same thermal energy storage capacity as the heat sink and PCM, however, it does not perceive the latent thermal energy absorption at a constant temperature. As a result, the temperatures after the melting range of the PCM are slightly higher for the numerical model compared to the experiment.

Fig. 6(b) shows the validation of the numerical model under vacuum conditions. The duration of the heating process in the experiments was 980 s for the case without PCM, and 1570 s for the case with PCM. The case without PCM presented a difference of 3.1 °C between the experimental and numerical data, observed in the first minutes of

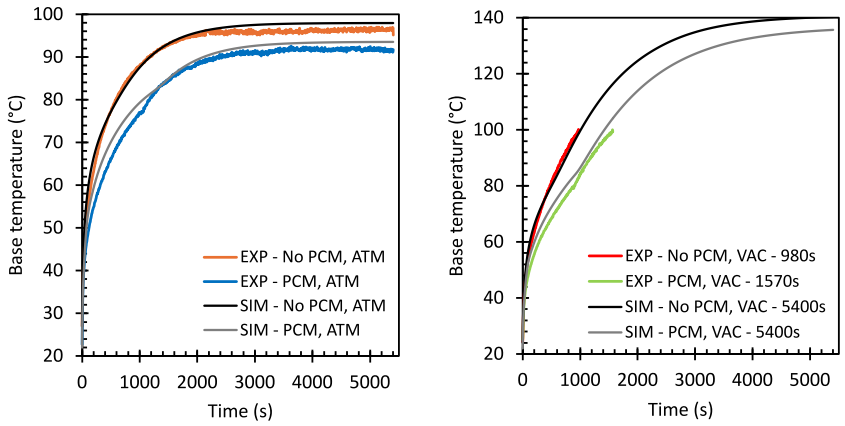

(a) ATM (b) VAC

Fig. 6. Validation of the simplified numerical model with the results from the experiments: base temperatures under atmospheric pressure (a) and vacuum (b). Maximum differences between model and experiment: (a) 4.2 °C for "No PCM", 4.7 °C for "PCM"; (b) 3.1 °C for "No PCM", 4.7 °C for "PCM".

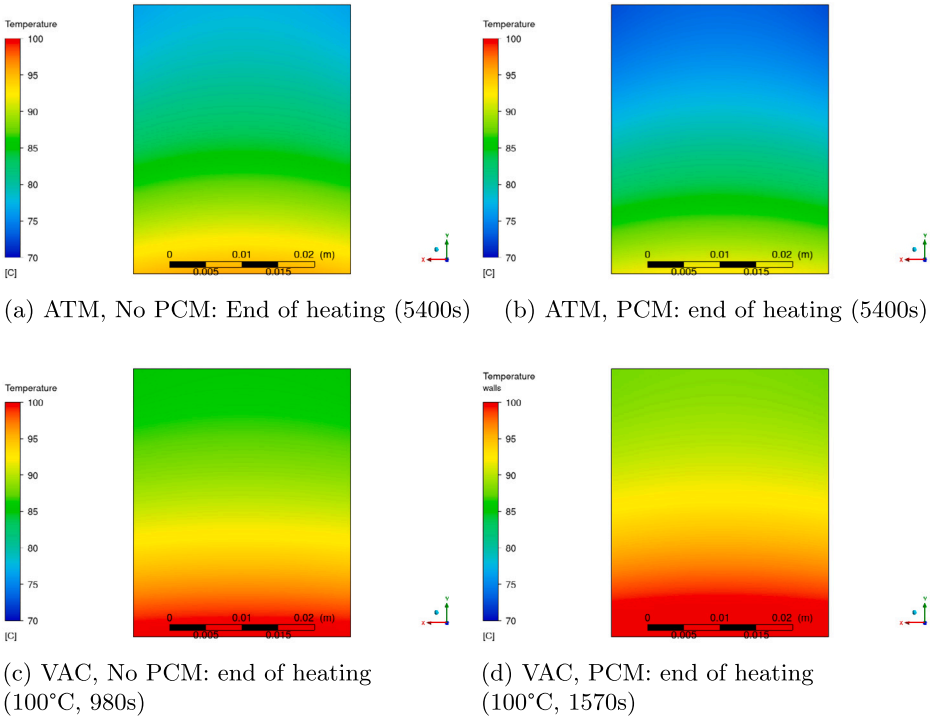

(a) ATM, No PCM: End of heating (5400s) (b) ATM, PCM: end of heating (5400s)

(c) VAC, No PCM: end of heating (100°C, 980s) (d) VAC, PCM: end of heating (100°C, 1570s)

Fig. 7. Temperature contours obtained from the reduced-order numerical model at the end of the heating process: 5400 s for atmospheric pressure without PCM (a) and with PCM (b), 980 s for vacuum without PCM (c), and 1570 s for vacuum with PCM (d). These plots illustrate top temperatures proportionally higher in vacuum than at atmospheric pressure at the end of the heating process.

heating. For the case with PCM, the maximum difference was 4.7 °C around the phase change region of the experiment. Further to the validation verification, both vacuum simulations were extrapolated to 5400 s heating to establish a direct comparison with the atmospheric pressure tests in Section 3.3. As can be observed in Fig. 6(b), the maximum base temperatures during the 5400 s heating are predicted to be around 140 °C for the case without PCM and around 135 °C for the case with PCM.

Overall, the reduced-order numerical model demonstrated a reasonable agreement with the experimental results. This validation supports its use as a tool for predicting the performance of heat sinks in both vacuum and atmospheric pressure environments.

Further verification of the applicability of this reduced order model as a predictor of the performance of thermal management modules, temperature contours at the end of the heating process were extracted from the simulations. Figs. 7(a) and 7(b) illustrate the wall temperature profile for the heat sinks in the absence and presence of PCM at atmospheric pressure, and the same for vacuum in Figs. 7(c) and 7(d). The duration of heating in the simulations mirrored the values obtained in the experimental tests. That is, the heating process was 5400 s long for both cases under atmospheric pressure, 980 s long for the no-PCM sample in vacuum, and 1570 s long for the case with PCM in vacuum. These temperature contour plots display considerably higher top temperatures in comparison to those observed in the experiments. The reason is due to the assembly of the free-hanging thermostat onto the top surface with tape, as described in Section 2.1.2. The noisy profiles of the top temperatures in the experimental graphs account for this discrepancy.

3.3. Cross-comparison: Atmospheric pressure vs. vacuum

This section compares the results for atmospheric pressure and vacuum conditions. The transient curves for both conditions are juxtaposed in Fig. 8 for comparison. Overall, the vacuum temperatures are higher

than those at atmospheric pressure due to the lack of convection heat transfer to the surroundings. In addition, the higher the power level, the greater the difference between atmospheric pressure and vacuum results.

The case without PCM is first analysed to establish the differences in performance under both environmental conditions. The maximum temperature at the base of the heat sink is compared for each power level across the heating period and summarised in Fig. 9. The maximum heating duration was set at 5400 s or until the base reached 100 °C, as previously explained. Both low and medium power tests completed the full 5400 s schedule. For low power, the maximum base temperature across the heating period was 50.0 °C in atmospheric pressure, and 65.2 °C in vacuum tests without PCM. Therefore, the maximum temperature achieved during heating is 25.4% higher in vacuum than at atmospheric pressure. For medium power, this figure is 32.8%. The high power test in atmosphere completed 5400 s of run time without PCM. In the vacuum high power test, the base temperature reached 100 °C after 980 s. To compare high power tests between atmosphere and vacuum, the reduced-order numerical simulation was extrapolated to 5400 s, as described in Section 3.2. The maximum temperature at the base of the heat sink for the atmospheric pressure experiment was 97.2 °C. For the extrapolated simulation in vacuum operation condition, the maximum temperature predicted across the 5400 s heating is 140 °C. Thus, the predicted maximum temperature in vacuum is 44% higher than at atmospheric pressure. This fits within the trend of higher power levels presenting higher differences between vacuum and atmospheric pressure temperatures.

In the case with PCM, the vacuum tests also displayed higher temperatures in comparison to atmospheric pressure tests, as displayed in Fig. 9. At low power, the base of the heat sink achieved a maximum temperature during the heating process 21.7% higher in vacuum. At medium power level, the maximum base temperature was 31.1% higher in vacuum. For the high power tests, the base of the heat sink reached 100 °C at 1570 s in vacuum, interrupting the heating process. Hence, the extrapolated simulation to 5400 s was also applied for the case with PCM to ensure a logical comparison with the atmospheric pressure test. During the 5400 s heating process, the atmospheric tests yielded a maximum base temperature of 92.5 °C. The maximum base temperature predicted in vacuum is 135 °C, which is 46% higher than in atmosphere.

The impact of PCM in lowering the electronics temperature is observed in the transient temperature graphs in Fig. 8 as the hatched area between the "No PCM" and "PCM" curves during the heating process. The vacuum results consistently present a larger hatched area across all power levels, indicating that the paraffin wax provides a greater improvement in electronics temperature in vacuum. The average and maximum differences in the base temperatures due to the presence of PCM are displayed in Fig. 10. The maximum difference was determined by comparing the "No PCM" and "PCM" temperatures at each time point during heating. The difference was most notable around the melting period of the PCM, during which the heating gradient decreases and the temperatures stabilise momentarily (Fig. 8(a)). At low power level, the addition of PCM improved the base temperature during the heating period by an average of 2.3 °C, or 4.7%, in atmospheric pressure and 4.8 °C, or 8.4%, in vacuum. For atmospheric pressure, the maximum improvement was 8.2%, at around 1130 s. For vacuum, PCM melted around 900 s, when the maximum difference between the "No PCM" and "PCM" curves was notes, at 11.3%. At medium power, while the maximum improvement caused by the PCM in the base temperatures was 7.4% for atmospheric pressure (at around 1840 s), it was 14.8% for vacuum (at 1550 s). On average, the difference between the "No PCM" and "PCM" curves was 2.7 °C, or 4.4% for atmospheric pressure, and 6.7 °C and 9.1% for vacuum. For the high power setting, the maximum enhancement by the PCM, which was also observed across the melting period, was 15.3% for atmospheric pressure and 18.5% for vacuum.

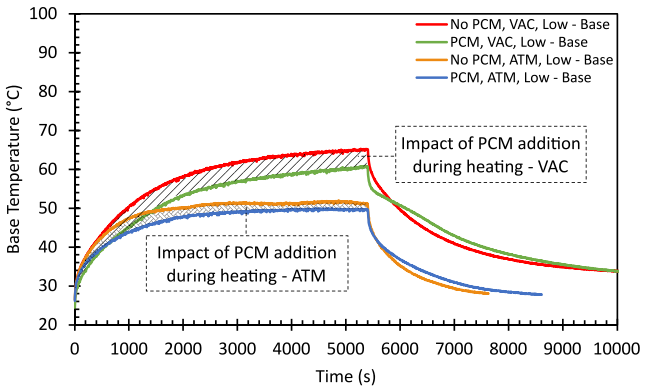

(a) ATM vs VAC - Low power

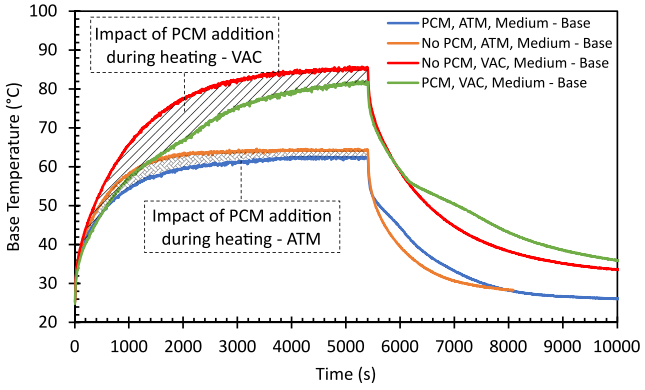

(b) ATM vs VAC - Medium power

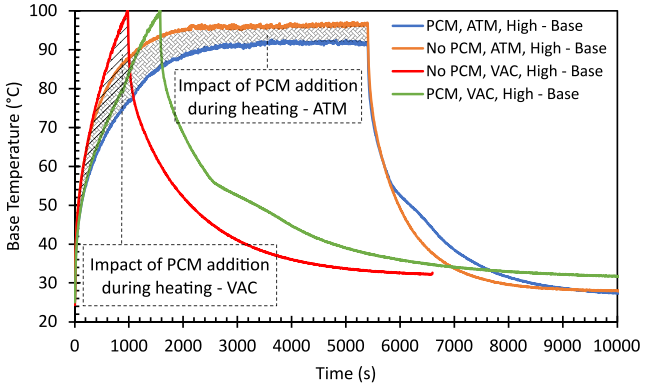

(c) ATM vs VAC - High power

Fig. 8. Transient temperatures for experiments conducted under atmospheric pressure and vacuum. Temperatures at the base and top surfaces of the heat sink at low (a), medium (b), and high (c) power levels.

The aim of utilising PCMs for thermal management of electronics is to prolong their operating time by keeping them under the maximum allowable working temperature. For this reason, the operating time, or the time to reach a determined set point temperature (SPT), is a commonly employed measure of the effectiveness of thermal management devices. Based on typical thermal design requirements for satellite electronic components [42,43], a SPT of 80.0 °C was adopted for comparison of their operating time in vacuum and under atmospheric pressure. Given the magnitude of the temperature, the comparison was done for high power level. With the data extracted from the transient graphs, Fig. 11 highlights that, in the absence of PCM, the electronics would operate for 590 s in atmospheric pressure conditions and 473 s

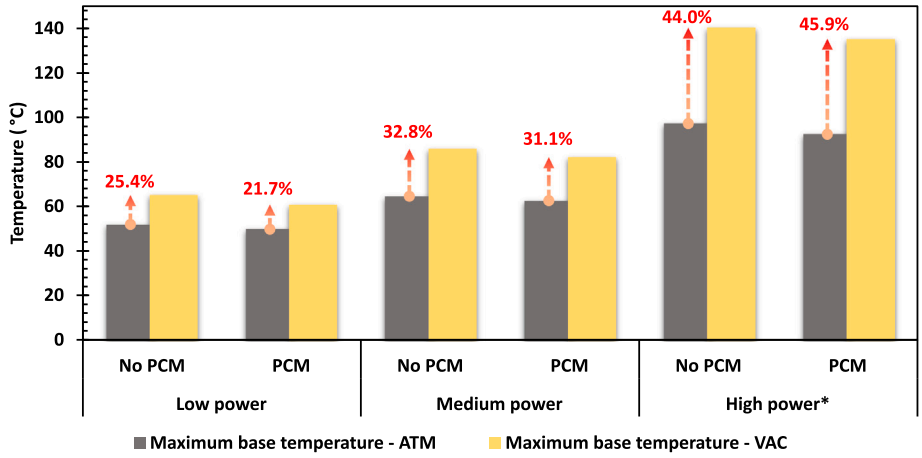

Fig. 9. Comparative of the maximum base temperatures achieved for the cases with and without PCM under atmospheric pressure and vacuum conditions during 5400 s heating process. * Maximum base temperatures for "No PCM" and "PCM" cases in vacuum were predicted through the reduced-order model simulation for 5400 s heating phase.

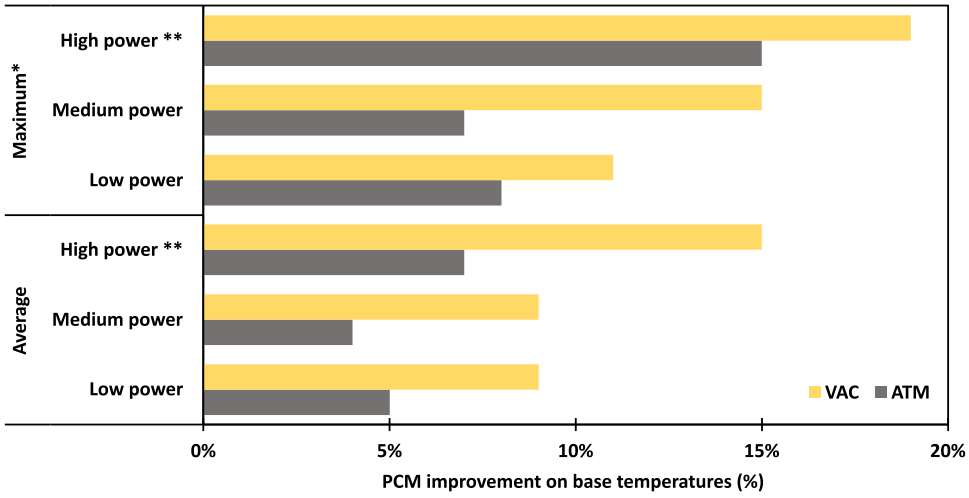

Fig. 10. PCM improvement in the maximum base temperatures under atmospheric pressure and vacuum conditions. *Around PCM melting phase **Heating process interrupted upon reaching 100 °C.

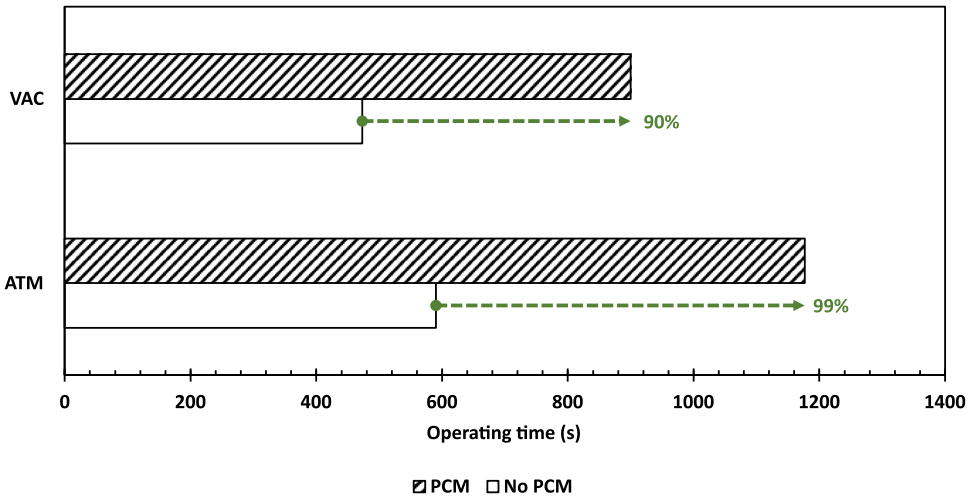

Fig. 11. PCM improvement in the electronics operating time to reach 80 °C under atmospheric pressure and vacuum conditions.

in vacuum. The presence of PCM almost doubles the operating time for both pressure conditions, more specifically an increase of 99% for atmospheric pressure (1177 s) and 90% for vacuum (900 s).

Based on the comparisons presented in this section, it may be concluded that there is a significant disparity in the performance of non-PCM and PCM-based thermal management modules under standard atmospheric and vacuum pressures. The addition of PCM into the thermal management module has a greater impact in lowering the electronics temperatures in vacuum than in atmosphere. This notes an important consideration for the design of thermal management modules for satellites.

4. Discussion

The first key difference in performance between vacuum and atmospheric pressure environments was that the base temperatures displayed in vacuum are higher than atmospheric pressure, regardless of the presence of PCM. This difference was expected due to the absence of convective heat transfer and therefore decreased heat dissipation from the heat sink. The base temperatures are as much as 33% higher in vacuum than at atmospheric pressure. It was observed that the higher the power level, the higher the temperature difference between atmospheric pressure and vacuum. This is supported by increased convection for higher temperatures at atmospheric pressure dominating radiative heat transfer.

The second key difference is that the effect of the addition of PCM in lowering the electronics temperatures is more evident in vacuum. Put differently, the reduction in the heat sink's base temperature from the addition of PCM was more pronounced under vacuum conditions. The maximum reduction in temperature is observed around the melting phase of the PCM. At medium power level, the maximum temperature reduction caused by the PCM was 11.2 °C, or 14.8%, in vacuum, as opposed to 4.6 °C, or 7.4%, in atmospheric pressure. This fact may be explained by the higher amount of thermal energy stored by the paraffin wax in vacuum due to the higher temperatures reached by the module in vacuum. The operation in vacuum yields not only higher temperatures at the base of the heat sink but also increases the temperatures throughout the entire module. We observe that in vacuum, the thermal gradient between the base and the top surfaces is diminished, meaning the temperature of the top surface is comparatively closer to the base temperature than at atmospheric pressure (Figs. 4 and 5). Therefore, these proportionally higher temperatures across the entire heat sink increase the thermal energy absorption by the PCM and, consequently, the relative benefit of PCM storage in lowering base temperatures is more evident. Proportionally higher temperatures across the heat sink's height and consequently higher thermal energy storage in vacuum may also explain the reason why paraffin wax phase change was observed at all power levels for vacuum, but only noticeable at medium and high power levels for atmospheric pressure tests.

The presence of PCM in the thermal management module was able to nearly double the operating time of electronics under both pressure conditions, which is very significant for satellite use. The operating time increased by 99% for atmospheric pressure and by 90% for vacuum. This comparison was done using a SPT of 80.0 °C and the high power setting. The similarity in the prolonged operating time for both pressure conditions may be attributed to the fact that the 80 °C set point temperature is slightly above the melting region for both conditions, indicating that PCM fusion at constant temperature took place instants prior to reaching the SPT. Therefore, at the time of reaching the SPT, the PCM had just melted on both cases, absorbing similar sensible and latent heat. Due to this increase in the operating time, it may be affirmed that the material properties of the selected PCM and its quantity are suitable for the proposed thermal management module at both operating conditions, considering high power operation and a maximum allowable temperature of 80.0 °C. The slightly greater effect of PCM in prolonging the operational time under atmospheric pressure is due to a longer melting period and consequently a longer period of stable temperatures, which increased the gap between the "No PCM" and "PCM" for atmospheric pressure, as evident in Fig. 8(c).

The simplified numerical model yielded coherent transient results in comparison to the experiments, as presented in Section 2.2. In addition, Fig. 7 confirms that the thermal gradient through the height of the heat sink is reduced in vacuum. The top surface temperatures obtained on the numerical results were higher than those in the experimental tests attributed to non-ideal contact between the surface and the free-hanging thermostat.

5. Conclusion

The study verified that, regardless of the presence or absence of PCM in the thermal management module, electronics operating in vacuum heat up more rapidly and sustain significantly higher temperatures than in atmospheric pressure due to the lack of convective heat transfer. The higher the power level, the larger the temperature difference observed between both pressure conditions. Electronics operation in vacuum displayed temperatures as much as 32.8% higher than at atmospheric pressure, hence why an effective thermal management strategy is critical for satellite applications.

The presence of PCM on the thermal management module demonstrated a greater impact on managing the electronics temperature in vacuum than at atmospheric pressure. The addition of PCM decreased the electronics temperatures by as much as 18.0 °C in vacuum, and by 12.3 °C in atmospheric temperature at high power level. Therefore implementing PCM-based thermal management modules as thermal management technique could effectively enhance the reliability of satellite electronics, as the reduction of just 1 °C in operating temperatures has been shown to decrease their failure rate by 4% [44,45].

Finally, the incorporation of PCM was also nearly doubled the electronics operating time under both pressure conditions at high power, which would be a significant benefit for thermal management modules in satellites. Given that most studies available in the literature have been conducted under atmospheric pressure conditions, the relevance of this work lies in investigating the performance of thermal management modules in vacuum, to support their design and optimisation for space applications.

Future research could explore the effect of different thermal conductivity enhancer designs and different materials, as well as incorporate a high-grade thermal vacuum chamber to reproduce orbit environments with higher fidelity.

CRediT authorship contribution statement

Laryssa Sueza Raffa: Writing – review & editing, Writing – original draft, Validation, Resources, Project administration, Methodology, Investigation, Formal analysis, Data curation, Conceptualization. **Matt Ryall:** Hardware, Software, Methodology. **Nick S. Bennett:** Writing – review & editing, Supervision. **Lee Clemon:** Writing – review & editing, Supervision, Investigation.

Declaration of competing interest

The authors declare the following financial interests/personal relationships which may be considered as potential competing interests: Laryssa Sueza Raffa reports financial support was provided by Australian Government. Nick Bennett reports financial support was provided by SmartSat Cooperative Research Council. If there are other authors, they declare that they have no known competing financial interests or personal relationships that could have appeared to influence the work reported in this paper.

Acknowledgements

This research was funded by SmartSat Cooperative Research Council, the University of Technology Sydney (UTS), and the Australian Government Research Training Program (RTP).

Appendix. Experimental data range

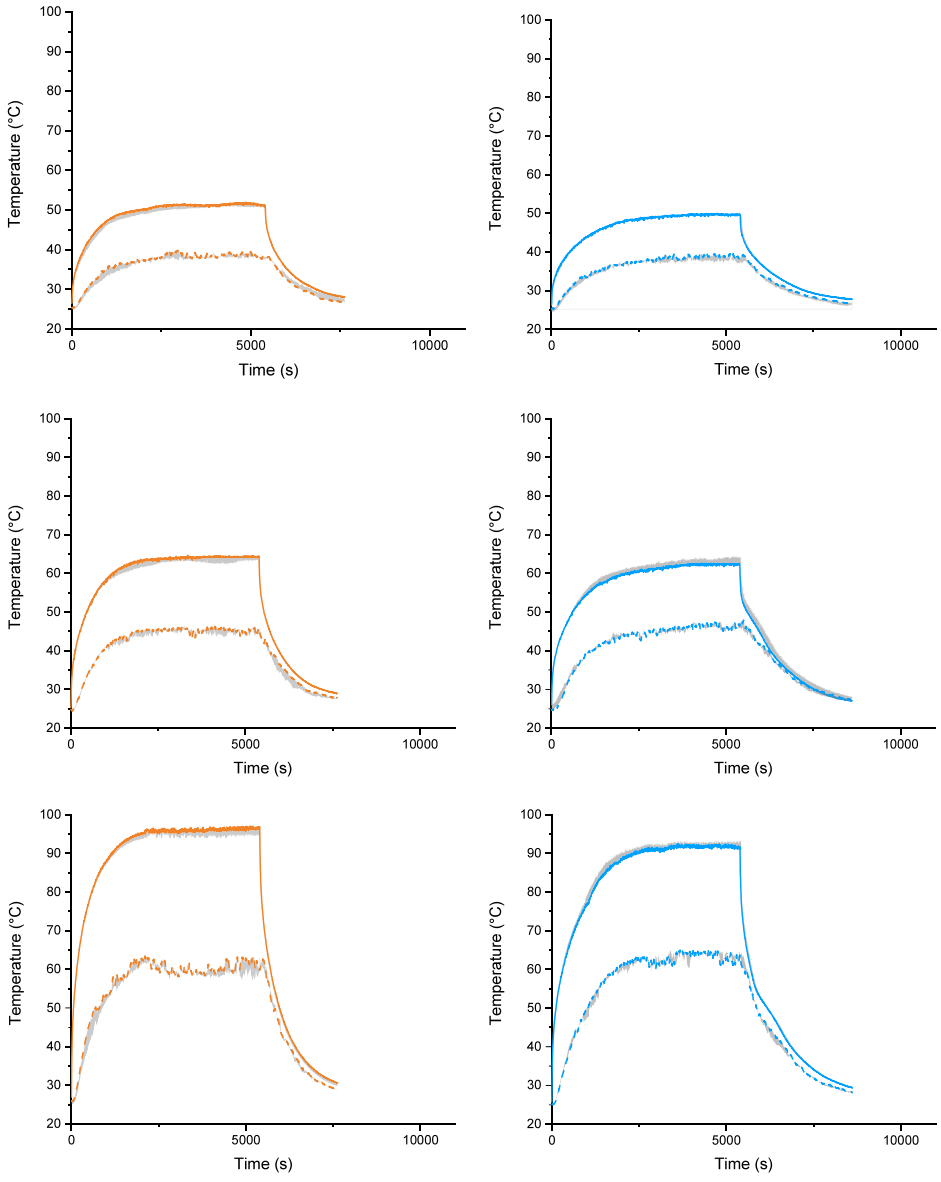

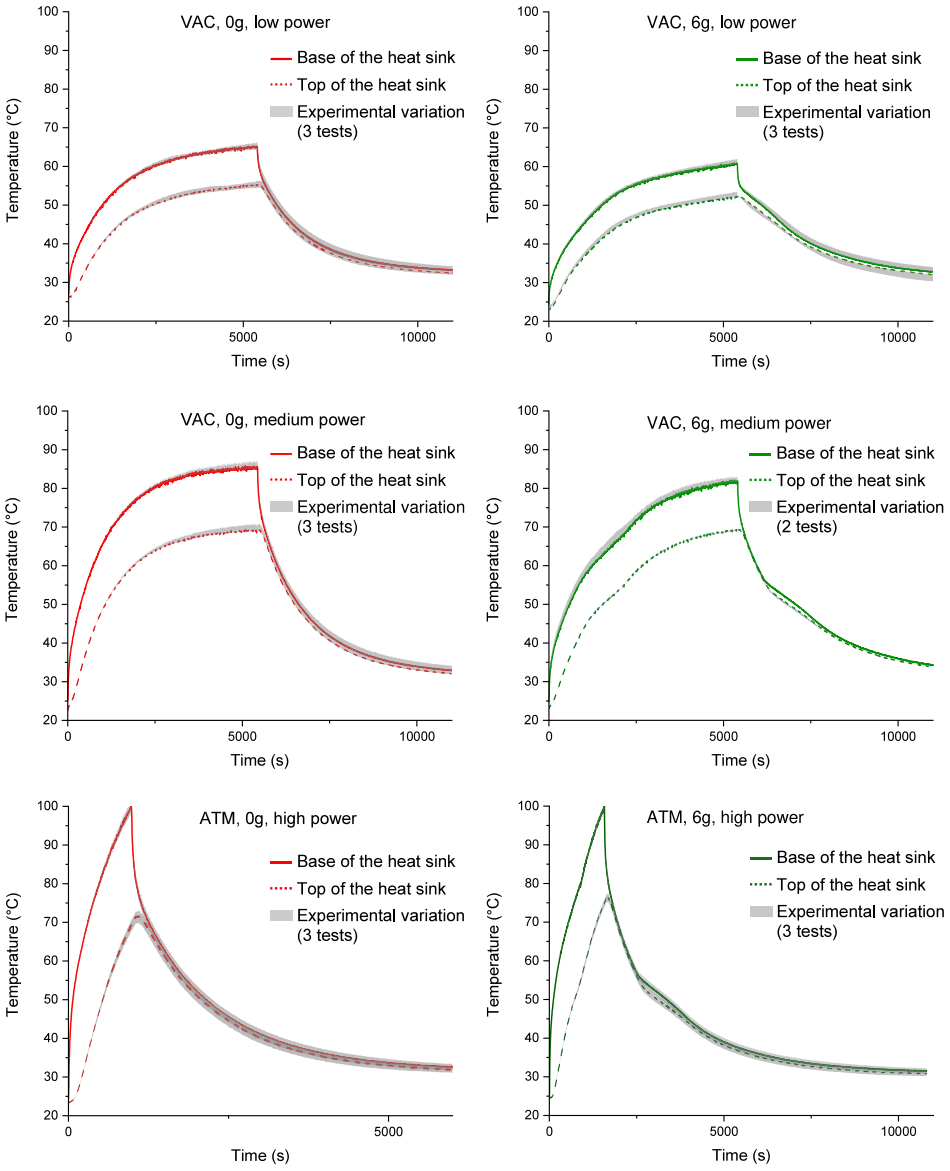

Data availability

Data will be made available on request.

References

[1] S. Selvadurai, A. Chandran, D. Valentini, B. Lamprecht, Passive thermal control design methods, analysis, comparison, and evaluation for micro and nanosatellites carrying infrared imager, Appl. Sci. 12 (6) (2022) 2858, http://dx.doi.org/10.3390/app12062858, URL https://www.mdpi.com/2076-3417/12/6/2858.

[2] D.S. Steinberg, Cooling Techniques for Electronic Equipment, second ed., Wiley, New York, 1991.

[3] R.J. McGlen, R. Jachuck, S. Lin, Integrated thermal management techniques for high power electronic devices, Appl. Therm. Eng. 24 (8–9) (2004) 1143–1156, http://dx.doi.org/10.1016/j.applthermaleng.2003.12.029, URL https://linkinghub.elsevier.com/retrieve/pii/S1359431104000316.

[4] K.K. Baraya, Thermal management challenges in small satellites, in: V.K. Singh, G. Choubey, S. Suresh (Eds.), Advances in Thermal Sciences, in: Lecture Notes in Mechanical Engineering, Springer Nature Singapore, Singapore, 2023, pp. 217–229, http://dx.doi.org/10.1007/978-981-19-6470-1_18, URL https://link.springer.com/10.1007/978-981-19-6470-1_18.

[5] D. Gilmore, Spacecraft Thermal Control Handbook, Volume I: Fundamental Technologies, American Institute of Aeronautics and Astronautics, Inc., Washington, DC, 2002, http://dx.doi.org/10.2514/4.989117, URL https://arc.aiaa.org/doi/book/10.2514/4.989117.

[6] J. Miao, Q. Zhong, Q. Zhao, X. Zhao, Spacecraft Thermal Control Technologies Space Science and Technologies Series Editor: Peijian Ye, Springer Nature Singapore, 2021, URL http://www.springer.com/series/16385.

[7] S. Tachikawa, H. Nagano, A. Ohnishi, Y. Nagasaka, Advanced passive thermal control materials and devices for spacecraft: A review, Int. J. Thermophys. 43, 91–92, http://dx.doi.org/10.1007/s10765-022-03010-3, (123). ISBN: 0123456789.

[8] K. Yamada, H. Nagano, Development of a heat storage panel for micro/nanosatellites and demonstration in orbit, Appl. Therm. Eng. 91 (2015) 894–900, http://dx.doi.org/10.1016/j.applthermaleng.2015.08.073, URL https://linkinghub.elsevier.com/retrieve/pii/S1359431115008698.

[9] H. Mahmud, D.H. Ahmed, Numerical investigations on melting of phase change material (PCM) with different arrangements of heat source-sink pairs under microgravity, Microgravity Sci. Technol. 34 (2) (2022) 20, http://dx.doi.org/10.1007/s12217-022-09936-5, URL https://link.springer.com/10.1007/s12217-022-09936-5.

[10] S. Wang, X. Hou, J. Yin, Y. Xing, Z. Wang, Comparative study of the thermal enhancement for spacecraft PCM thermal energy storage units, Aerospace 9 (11)

(2022) 705, http://dx.doi.org/10.3390/aerospace9110705, URL https://www.mdpi.com/2226-4310/9/11/705.
[11] W.-f. Wu, N. Liu, W.-l. Cheng, Y. Liu, Study on the effect of shape-stabilized phase change materials on spacecraft thermal control in extreme thermal environment, Energy Convers. Manage. 69 (2013) 174–180, http://dx.doi.org/10.1016/j.enconman.2013.01.025, URL https://linkinghub.elsevier.com/retrieve/pii/S0196890413000691.
[12] S. Mahmoud, Experimental investigation of inserts configurations and PCM type on the thermal performance of PCM based heat sinks, Appl. Energy (2013).
[13] H. Nazir, M. Batool, F.J. Bolivar Osorio, M. Isaza-Ruiz, X. Xu, K. Vignarooban, P. Phelan, Inamuddin, A.M. Kannan, Recent developments in phase change materials for energy storage applications: A review, Int. J. Heat Mass Transfer 129 (2019) 491–523, http://dx.doi.org/10.1016/j.ijheatmasstransfer.2018.09.126, URL https://linkinghub.elsevier.com/retrieve/pii/S0017931018324578.
[14] J. Pereira Da Cunha, P. Eames, Thermal energy storage for low and medium temperature applications using phase change materials – A review, Appl. Energy 177 (2016) 227–238, http://dx.doi.org/10.1016/j.apenergy.2016.05.097, URL https://linkinghub.elsevier.com/retrieve/pii/S0306261916306948.
[15] J. Hu, R. Hu, C. Yuan, B. Duan, M. Huang, X. Luo, Fabrication and thermal characterization of the modularized thermal storage unit, IEEE Trans. Compon. Packag. Manuf. Technol. (2016) 1–10, http://dx.doi.org/10.1109/TCPMT.2016.2582503, URL http://ieeexplore.ieee.org/document/7508378/.
[16] K. Nayak, S. Saha, K. Srinivasan, P. Dutta, A numerical model for heat sinks with phase change materials and thermal conductivity enhancers, Int. J. Heat Mass Transfer 49 (11–12) (2006) 1833–1844, http://dx.doi.org/10.1016/j.ijheatmasstransfer.2005.10.039, URL https://linkinghub.elsevier.com/retrieve/pii/S0017931005006824.
[17] K. Swaminathan Gopalan, V. Eswaran, Numerical investigation of thermal performance of PCM based heat sink using structured porous media as thermal conductivity enhancers, Int. J. Therm. Sci. 104 (2016) 266–280, http://dx.doi.org/10.1016/j.ijthermalsci.2016.01.008, URL https://linkinghub.elsevier.com/retrieve/pii/S1290072916000168.
[18] H. Bashirpour-Bonab, Investigation and optimization of PCM melting with nanoparticle in a multi-tube thermal energy storage system, Case Stud. Therm. Eng. 28 (2021) 101643, http://dx.doi.org/10.1016/j.csite.2021.101643, URL https://linkinghub.elsevier.com/retrieve/pii/S2214157X21008066.
[19] P. Bose, V.A. Amirtham, A review on thermal conductivity enhancement of paraffinwax as latent heat energy storage material, Renew. Sustain. Energy Rev. 65 (2016) 81–100, http://dx.doi.org/10.1016/j.rser.2016.06.071, URL https://linkinghub.elsevier.com/retrieve/pii/S1364032116303033.
[20] W. Ye, D. Jamshideasli, J.M. Khodadadi, Improved performance of latent heat energy storage systems in response to utilization of high thermal conductivity fins, Energies 16 (3) (2023) 1277, http://dx.doi.org/10.3390/en16031277, URL https://www.mdpi.com/1996-1073/16/3/1277.
[21] S. Zhang, S. Mancin, L. Pu, A review and prospective of fin design to improve heat transfer performance of latent thermal energy storage, J. Energy Storage 62 (2023) 106825, http://dx.doi.org/10.1016/j.est.2023.106825, URL https://linkinghub.elsevier.com/retrieve/pii/S2352152X23002220.
[22] R. Pakrouh, M. Hosseini, A. Ranjbar, R. Bahrampoury, A numerical method for PCM-based pin fin heat sinks optimization, Energy Convers. Manage. 103 (2015) 542–552, http://dx.doi.org/10.1016/j.enconman.2015.07.003, URL https://linkinghub.elsevier.com/retrieve/pii/S0196890415006548.
[23] M.J. Ashraf, H.M. Ali, H. Usman, A. Arshad, Experimental passive electronics cooling: Parametric investigation of pin-fin geometries and efficient phase change materials, Int. J. Heat Mass Transfer 115 (2017) 251–263, http://dx.doi.org/10.1016/j.ijheatmasstransfer.2017.07.114, URL https://linkinghub.elsevier.com/retrieve/pii/S0017931017313017.
[24] A. Tavakoli, J. Hashemi, M. Najafian, A. Ebrahimi, Physics-based modelling and data-driven optimisation of a latent heat thermal energy storage system with corrugated fins, Renew. Energy 217 (2023) 119200, http://dx.doi.org/10.1016/j.renene.2023.119200, URL https://linkinghub.elsevier.com/retrieve/pii/S0960148123011151.
[25] J. Xie, K.F. Choo, J. Xiang, H.M. Lee, Characterization of natural convection in a PCM-based heat sink with novel conductive structures, Int. Commun. Heat Mass Transfer 108 (2019) 104306, http://dx.doi.org/10.1016/j.icheatmasstransfer.2019.104306, URL https://linkinghub.elsevier.com/retrieve/pii/S0735193319301721.
[26] R. Baby, C. Balaji, Experimental investigations on phase change material based finned heat sinks for electronic equipment cooling, Int. J. Heat Mass Transfer 55 (5–6) (2012) 1642–1649, http://dx.doi.org/10.1016/j.ijheatmasstransfer.2011.11.020, URL https://linkinghub.elsevier.com/retrieve/pii/S0017931011006570.
[27] R. Baby, C. Balaji, Thermal optimization of PCM based pin fin heat sinks: An experimental study, Appl. Therm. Eng. 54 (1) (2013) 65–77, http://dx.doi.org/10.1016/j.applthermaleng.2012.10.056, URL https://linkinghub.elsevier.com/retrieve/pii/S1359431113000045.
[28] G. Schmid, L.-H. Yang, T.-H. Yang, S.-L. Chen, Influence of inter-fin base length on thermal performance of free hanging horizontal base heat sinks, Appl. Therm. Eng. 108 (2016) 1226–1236, http://dx.doi.org/10.1016/j.applthermaleng.2016.08.034, URL https://linkinghub.elsevier.com/retrieve/pii/S1359431116313801.
[29] S. Hosseinizadeh, F. Tan, S. Moosania, Experimental and numerical studies on performance of PCM-based heat sink with different configurations of internal fins, Appl. Therm. Eng. 31 (17–18) (2011) 3827–3838, http://dx.doi.org/10.1016/j.applthermaleng.2011.07.031, URL https://linkinghub.elsevier.com/retrieve/pii/S1359431111003905.
[30] A. Arshad, M. Ibrahim Alabdullatif, M. Jabbal, Y. Yan, Towards the thermal management of electronic devices: A parametric investigation of finned heat sink filled with PCM, Int. Commun. Heat Mass Transfer 129 (2021) 105643, http://dx.doi.org/10.1016/j.icheatmasstransfer.2021.105643, URL https://linkinghub.elsevier.com/retrieve/pii/S0735193321005364.
[31] M. Arqam, L.S. Raffa, L. Clemon, M.S. Islam, M. Ryall, N.S. Bennett, Numerical and experimental investigation of a phase change material radial fin heat sink for electronics cooling, J. Energy Storage 98 (2024) 113113, http://dx.doi.org/10.1016/j.est.2024.113113, URL https://linkinghub.elsevier.com/retrieve/pii/S2352152X24026999.
[32] Y. Guo, H. Yang, G. Lin, H. Jin, X. Shen, J. He, J. Miao, Thermal performance of a 3D printed lattice-structure heat sink packaging phase change material, Chin. J. Aeronaut. 34 (5) (2021) 373–385, http://dx.doi.org/10.1016/j.cja.2020.07.033, URL https://linkinghub.elsevier.com/retrieve/pii/S1000936120303551.
[33] A.M. Elshaer, A. Soliman, M. Kassab, A. Hawwash, Experimental and numerical investigations of an open-cell copper foam (OCCF)/phase change material (PCM) composite-based module for satellite avionics thermal management in a thermal vacuum chamber (TVC), J. Energy Storage 75 (2024) 109572, http://dx.doi.org/10.1016/j.est.2023.109572, URL https://linkinghub.elsevier.com/retrieve/pii/S2352152X23029705.
[34] A.M. Elshaer, A. Soliman, M. Kassab, S. Mori, A. Hawwash, Numerical study about thermal performance evaluation of PCM and PCM/fins composite-based thermal control module at microgravity conditions, Int. J. Thermofluids 20 (2023) 100419, http://dx.doi.org/10.1016/j.ijft.2023.100419, URL https://linkinghub.elsevier.com/retrieve/pii/S2666202723001350.
[35] K. Kansara, V. Singh, R. Patel, R. Bhavsar, A. Vora, Numerical investigations of phase change material (PCM) based thermal control module (TCM) under the influence of low gravity environment, Int. J. Heat Mass Transfer 167 (2021) 120811, http://dx.doi.org/10.1016/j.ijheatmasstransfer.2020.120811, URL https://linkinghub.elsevier.com/retrieve/pii/S0017931020337492.
[36] A.M. Elshaer, A. Soliman, M. Kassab, A. Hawwash, The effect of melting point and combination of phase change materials on the thermal control performance of small satellites in the thermal environment of low earth orbit: Numerical study, J. Energy Storage 59 (2023) 106531, http://dx.doi.org/10.1016/j.est.2022.106531, URL https://linkinghub.elsevier.com/retrieve/pii/S2352152X22025208.
[37] E. Alawadhi, C. Amon, PCM thermal control unit for portable electronic devices: Experimental and numerical studies, IEEE Trans. Compon. Packag. Technol. 26 (2003) 116–125, http://dx.doi.org/10.1109/TCAPT.2003.811480.
[38] H. Ye, H. He, X. Ge, B. Xu, Comparative numerical investigations on the melting process of form-stable phase change material using enthalpy formulation method and effective heat capacity formulation method, Taiyangneng Xuebao/Acta Energiae Solaris Sinica 25 (2004) 488–491.
[39] Sigma-Aldrich, Sigma-Aldrich product specification: Paraffin wax 327204, 2024, URL https://www.sigmaaldrich.com/specification-sheets/325/952/327204-BULK____ALDRICH_.pdf.
[40] G. Mohr, S. Nowakowski, S.J. Altenburg, C. Maierhofer, K. Hilgenberg, Experimental determination of the emissivity of powder layers and bulk material in laser powder bed fusion using infrared thermography and thermocouples, Metals 10 (11) (2020) 1546, http://dx.doi.org/10.3390/met10111546, URL https://www.mdpi.com/2075-4701/10/11/1546.
[41] A. Arshad, M. Jabbal, P.T. Sardari, M.A. Bashir, H. Faraji, Y. Yan, Transient simulation of finned heat sinks embedded with PCM for electronics cooling, Therm. Sci. Eng. Prog. 18 (2020) 100520, http://dx.doi.org/10.1016/j.tsep.2020.100520, URL https://linkinghub.elsevier.com/retrieve/pii/S245190492030041X.
[42] S.-J. Kang, H.-U. Oh, On-orbit thermal design and validation of 1 U standardized CubeSat of STEP cube lab, Int. J. Aerosp. Eng. 2016 (2016) 1–17, http://dx.doi.org/10.1155/2016/4213189, URL http://www.hindawi.com/journals/ijae/2016/4213189/.
[43] R. Kandasamy, X.-Q. Wang, A.S. Mujumdar, Transient cooling of electronics using phase change material (PCM)-based heat sinks, Appl. Therm. Eng. 28 (8–9) (2008) 1047–1057, http://dx.doi.org/10.1016/j.applthermaleng.2007.06.010, URL https://linkinghub.elsevier.com/retrieve/pii/S1359431107002116.
[44] Z. Wan, G. Guo, K. Su, Z. Tu, W. Liu, Experimental analysis of flow and heat transfer in a miniature porous heat sink for high heat flux application, Int. J. Heat Mass Transfer 55 (15–16) (2012) 4437–4441, http://dx.doi.org/10.1016/j.ijheatmasstransfer.2012.04.013, URL https://linkinghub.elsevier.com/retrieve/pii/S0017931012002566.
[45] G.N. Morrison, J.M. Kallis, L.A. Strattan, I.R. Jones, A.L. Lena, RADC Thermal Guide for Reliability Engineers, Tech. Rep. RADC-TR-82-172, Air Force Systems Command, Griffith Air Force Base, Rome Air Development Centre, New York, 1982, URL https://apps.dtic.mil/sti/pdfs/ADA118839.pdf.